# Structural, electronic, optical and thermoelectric analysis of Rb/Cs2TeBr6 Vacancy ordered double perovskites

**Malak Azmat Ali** ( azmatupesh@gmail.com )

Government Post Graduate Jahanzeb College Saidu Sharif, Swat 19130, Khyber Pakhtunkhwa, Pakistan

**G. Murtaza**

Islamia College Peshawar 25120, Khyber Pakhtunkhwa, Pakistan

**Research Article**

**Keywords:** vacancy ordered double perovskites, optical conductivity, solar cell, figure of merit, Seebeck coefficient

**Posted Date:** April 3rd, 2021

**DOI:** https://doi.org/10.21203/rs.3.rs-379113/v1

# Structural, electronic, optical and thermoelectric analysis of $Rb/Cs_2TeBr_6$ Vacancy ordered double perovskites

Malak Azmat Ali[1], G. Murtaza[2, 3]

[1]*Department of Physics, Government Post Graduate Jahanzeb College Saidu Sharif, Swat 19130, Khyber Pakhtunkhwa, Pakistan*

[3]*Materials Modeling Lab, Department of Physics, Islamia College Peshawar 25120, Khyber Pakhtunkhwa, Pakistan*

[3]*Department of Mathematics & Natural sciences, Prince Mohammad Bin Fahd University, P. O. Box 1664, Alkhobar 31952, Kingdom of Saudi Arabia*

e-mail: azmatupesh@gmail.com

**Abstract**

It is compulsory to develop technologies able to generate energy at negligible cost to the environment. Therefore, in present work, lead free vacancy ordered double perovskites $Rb/Cs_2TeBr_6$ were reported as green energy materials on basis of full potential linearized augmented plane wave method calculations. The study has been carried out in terms of structural, electronic, optical and thermoelectric properties. It was noted from values of tolerance factor and formation energy that both $Rb/Cs_2TeBr_6$ compounds are stable in perovskite structure. The band gaps were calculated in close resemblance with experiments. These values (2.09 eV $Rb_2TeBr_6$ and 2.10 eV for $Cs_2TeBr_6$ with EV-GGA) were examined in visible range of electromagnetic spectrum. The optical properties such as real and imaginary parts of dielectric function, optical conductivity and reflectivity ensured the use of $Rb/Cs_2TeBr_6$ compounds for solar cell applications. Also, the reasonable values of Seebeck coefficients and figure of merit proposed the studied compounds for thermoelectric power generation.

**Keywords:** vacancy ordered double perovskites; optical conductivity; solar cell; figure of merit; Seebeck coefficient

## 1. Introduction

Presently, our earth's atmosphere is facing with rapid increase in greenhouse gases due to extensive use of fossil fuels for energy application. This causes unusual changes in climate, as result weathers are becoming more intensive. Therefore, it is necessary to develop technologies able to generate energy at negligible cost to the environment. Producing energy through solar cells is considered one of the cheaper options to provide very clean and cheap energy [**1**]. In this perspective, lead halide perovskites are recognized as best photovoltaic materials [**2-3**]. This class achieved solar energy conversion efficiency more than 25 % [**4]** due to high mobility of charge carriers, large absorption coefficients [**5**] and large carrier diffusion length [**6**]. Recently, lead halide perovskites were also reported as excellent materials for thermoelectric power generation [**7-13**]. Where, a gradient of temperature across these materials can causes motion of free charge carriers and generate a voltage [**10**]. Regardless of multifunctional character of lead halide perovskites, it is important that improved version of the next common solar cell materials must be lead free, economical and environmental friendly.

Vacancy ordered double perovskites, were widely studied as alternative of lead perovskites. As result, compounds of this class were proven as good conductors and have been considered as solar cell absorbers [**14-19**].This group of compounds is generally represented by $A_2BX_6$, where, A, B are cations, and X is a halide [**20**]. The structure of $A_2BX_6$ compounds has close similarity to the structure of cubic perovskite $ABX_3$ with half of the B sites cation removed in an organized method. $Rb_2TeBr_6$ and $Cs_2TeBr_6$ prepared with $A_2BX_6$ structure are still required to be exposed completely from theoretical point of view for possible applications. These compounds were

extensively studied for structural properties at experimental and theoretical sides [**21-25**]. Peresh et al. [**26**] calculated band gap of $Rb_2TeBr_6$ and $Cs_2TeBr_6$ as 2.14 and 2.12 eV from their experiments. These band gaps lie within visible range of electromagnetic spectrum [**27**]. Therefore, $Rb_2TeBr_6$ and $Cs_2TeBr_6$ compounds should be studied for solar cell applications. Also, thermoelectric properties of these materials must be predicted to guide future experiments.

In this article, I report my full potential linearized augmented plane wave method calculated results of structural, electronic, optical and thermoelectric properties of Rb/$Cs_2TeBr_6$ with physical insight. I hope that my calculations will motivate the experimenters to carry further analysis of these compounds for solar cells and thermoelectric generators and will cover missing theoretical data in literature.

## 2. Research Techniques

### 2.1 Computational Details

In present work, simulations were performed with the Wien2k code of full potential linearized augmented plane wave method [**28**]. The exchange correlation function was treated with generalized gradient approximation of Wu-Cohen (WC-GGA) [**29**] and Engle –Vosko (EV-GGA) [**30**]. Also WC-GGA Coupled modified Beck Johnson (MBJ) [**31**] was taken in calculation of electronic properties. The thermoelectric properties were computed within classical transport theory integrated in BoltzTrap code [**32**].

### 2.2 Convergence study

The energy within self-consistent field (SCF) was converged using the product of cut-off wave factor ($K_{max}$) with smallest muffin-tin radii (RMT) as 7, the upper limit value to angular momentum vector ($l_{max}$) as 12 and k points mesh as 7 × 7 × 7 within Monkhorst and Pack [**33**]. These values ensured balance computational accuracy and calculation time. The atomic radii

($R_{MT}$) of for Rb, Cs, Te and Br were taken as 2.5, 2.5, 2.4, 2.34 a.u as result of internal structure optimization. Also, the positions of atoms listed in **Table 1** were obtained after optimization of internal structure.

### 2.3 Materials

This research focus on lead free vacancy ordered double perovskites $Rb_2TeBr_6$ and $Cs_2TeBr_6$. These are important research compounds due to their small cost in both and environmental and financial terms. The vacancy ordered double perovskites family has cubic conventional unit cell (having four formula units) with nine atoms in each formula unit as shown in **Fig. 1**. The structure of these compounds is often described as consisting of isolated $[TBr_6]^{2-}$ octahedral [**34**] with monovalent Rb/Cs site cations to balance charge.

## 3. Results and Discussions

### 3.1 Structure properties

Experimentally, $Rb_2TeBr_6$ and $Cs_2TeBr_6$ were found to be stable in cubic phase with Fm-3m space group. To check stability theoretically, the tolerance factors (t) were calculated via below equation [**35**]

$$t = \frac{r_{Br}}{r_{Te}} - n_{Rb/Cs}\left(n_{\frac{Rb}{Cs}} - \frac{{}^{r_{Rb/Cs}}/_{r_{Te}}}{\ln({}^{r_{Rb/Cs}}/_{r_{Te}})}\right) \qquad (1)$$

Here, $r_{Te}$, $r_{Rb/Cs}$ and $r_{Br}$ are ionic radii Te, Rb/Cs and Br atoms, respectively. Taking the values of these radii from [**24**], the values of t were calculated as 4.12 and 3.95 for $Rb_2TeBr_6$ and $Cs_2TeBr_6$. By definition, t<4.18 indicate cubic perovskites [**35**]. Therefore, it is proved that studied compounds are stable in cubic perovskites phase.

Now to find formation energy, E (F) of Rb/$Cs_2TeBr_6$ compounds the following equation has been used [**17**]

$$E\,(F) = E(Rb/Cs_2TeBr_6) - 2\,(E_{Cs/Rb}) - (E_{Te}) - 6(E_{Br}) \qquad (2)$$

Here in eq. 2, $E(Rb_2/Cs_2TeBr_6)$ is the total energy of $Rb_2TeBr_6$ or $Cs_2TeBr_6$, and $E_{Cs/Rb}$, $E_{Te}$ and $E_{Br}$ are the energies of constituent atoms in $Rb/Cs_2TeBr_6$ compounds. All these values are given in **Table 2**. The negative values of calculated E (F) in the table indicate the formation reaction of studied compounds is exothermic. The compounds formed through exothermic reaction are considered to be stable [**36**]. Therefore, $Rb/Cs_2TeBr_6$ compounds remains stable after formation.

After confirmation of cubic phase stability with perovskite structure, the lattice parameters were calculated by volume optimization process by force field approximation (**Fig. 2**) followed by fitting the obtained date in Birch-Murnaghan equation [**37**]. The WC-GGA was used as exchange correlation function for optimization process. The calculated parameters were assembled in **Table 3** with corresponding data available in literature. The values of lattice constant are in reasonable agreement with the available experimental and theoretical values. However, these values are little overestimated from experimental values. This overestimation is common trend in GGA calculations [**38**]. Since, the values of bulk modulus are unavailable. My calculated values will be reference for future works. However, these values follow common trend [**39-40**] of decreasing as the cation go down the group (Rb to Cs).

**3.2 Electronic properties**

The electronic properties of $Rb/Cs_2TeBr_6$ compounds were calculated using WC-GGA, EV-GGA and MBJ**.** Band structure calculated through these exchange correlation potential are depicted in **Fig. 3** and the corresponding values of band gap are grouped in **Table 4** along with available experimental values. These band structures were plotted in Gnuplot by considering point sampling as Γ (0, 0, 0), L ($\frac{1}{2}$, $\frac{1}{2}$, $\frac{1}{2}$), X ($\frac{1}{2}$, 0, $\frac{1}{2}$) and W ($\frac{1}{2}$, $\frac{1}{4}$, $\frac{3}{4}$) in reciprocal lattice. The

maximum of valence band of both the Rb/$Cs_2TeBr_6$ compounds lie at W while the minimum of conduction band lies at L symmetry point. Therefore, the studied compounds are indirect band gap materials in W→L direction. The band gap ($E_g$) values in **Table 4** follow the order as $E_g$ (WC-GGA) < $E_g$ (EV-GGA) < $E_g$ (MBJ). However, $E_g$ values through EV-GGA are in close resemblance with experimental values [**26**]. Therefore, I will use these values for calculation of optical and thermoelectric properties. It worth to note that band gap values lies with visible range of electromagnetic spectrum. It is expected that Rb/$Cs_2TeBr_6$ may be used effectively for solar cell applications.

**Fig. 4** shows the DOS calculated via EV-GGA because DOS calculated through WC-GGA, EV-GGA and MBJ has similar nature. To explain the figure, electronic configurations of Rb, Cs, Te and Br were treated as [Kr]$5s^1$, [Xe]$6s^1$, [Ar]$4d^{10}5s^25p^4$ and [Ar]$3d^{10}4s^24p^5$. The valence band maximum of both the compounds is composed of completely filled Te-$5s^2$ states and partially filled Br-$4p^5$ (as they are contributed from 0 to -3 eV) states. Where, conduction band minimum is contributed from partially filled $5p^4$ states of Te. Therefore, the energy difference between these states defines band gap and fundamental transition predict p-type conductivity in both the Rb/$Cs_2TeBr_6$ compounds. The distribution of the states toward remaining valence and conduction band can be observed from the **Fig. 4**.

### 3.3 Optical properties

The optical properties depend upon band gap ($E_g$) of a material. As $E_g$ defines the absorption edge. The calculated band gap of Rb/$Cs_2TeBr_6$ is 2.09/2.10 eV with EV-GGA. A material having band gap in range of 1.8-3.1 eV are considered to have excellent optical properties for solar cells applications. Therefore, to check fitness of Rb/$Cs_2TeBr_6$ vacancy ordered perovskites, I have calculated the optical properties in term of real and imaginary parts of dielectric function ($\varepsilon_1(\omega)$

and $\varepsilon_2(\omega)$), optical conductivity ($\sigma(\omega)$) and reflectivity ($R(\omega)$) in energy range of 0-6 eV and depicted in **Fig. 5**. Where, blue and black solid lines are representative of optical parameters of $Rb_2TeBr_6$ and $Cs_2TeBr_6$, respectively.

Since, $Rb/Cs_2TeBr_6$ perovskites have cubic structure as described above, the linear dielectric tensor has only one components $\varepsilon(\omega) = \varepsilon_1(\omega) + \iota\, \varepsilon_2(\omega)$ [**41**]. The **Fig 5 (a)** shows the calculated real part, $\varepsilon_1(\omega)$. $\varepsilon_1(\omega)$ demonstrates the extent to which a material gets polarized when exposed to electromagnetic radiation. This function gets started from static value $\varepsilon_1(0)$. This $\varepsilon_1(0)$ is related with band gap of a material by Penn's model [**42**]

$$\varepsilon_1(0) \approx 1 + \left(\hbar\omega_P / E_g\right)^2 \qquad (3)$$

As discussed earlier that both the studied compounds have nearly equal band gaps. This results nearly equal value of $\varepsilon_1(0)$. Beyond $\varepsilon_1(0)$, $\varepsilon_1(\omega)$ get increases to maximum value $(\varepsilon_1(\omega))_{Max}$ and then starts decreasing and enter to negative values. The photons having energy in the region of negative value get reflected when incident on $Rb/Cs_2TeBr_6$ compounds and the optical nature of materials shifts to metallic region [**43**]. The $\varepsilon_1(\omega)$ is only distinguishable for $Rb/Cs_2TeBr_6$ in energy range of 4-6 eV. This may be attributed to nearly same band structures of $Rb/Cs_2TeBr_6$ compounds.

The real part of dielectric function $\varepsilon_2(\omega)$ reflects the absorption behavior of a material. Its value starts at energy nearly equal to band gap because the transfer of charge carriers between conduction and valence bands initiates as clear from **Fig. 5 (a)**. The maximum peak values of $\varepsilon_2(\omega)$ are around 2.9 eV for both the $Rb/Cs_2TeBr_6$ compounds. The origin of this peak is attributed by interband transition from partially filled $5p^4$ states of Te to and partially filled Br-$4p^5$ states. The maximum absorption occurs in visible region of electromagnetic spectrum. Therefore, both the $Rb/Cs_2TeBr_6$ compounds are best for solar cell fabrication.

The frequency dependent optical conductivity σ(ω) displayed in **Fig 5 (c)** has similar behavior as $\varepsilon_2(\omega)$. Because, photon absorbed by charges cause transitions and results optical conductivity. The maximum σ(ω) of Rb/$Cs_2TeBr_6$ compounds has nearly same values as seen from the figure. It occurs when the incident photon energy becomes 2.9 eV. Beyond this energy limit, σ(ω) gets decrease in ultraviolet region of electromagnetic spectrum.

The calculated reflectivity R(ω) of Rb/$Cs_2TeBr_6$ compounds is illustrated in **Fig 5 (d)**, where, the zero frequency limit is less than is 15 % for both perovskites. With increase of incident photon energy, R(ω) gets increase and reaches at maximum value of 40 % in ultra violet energies. In this region negative values of $\varepsilon_1(\omega)$ were recorded., In this energy range, the absorption behavior becomes decreased and Rb/$Cs_2TeBr_6$ compounds response as metals to the incident photons.

**3.4 Thermoelectric properties**

The Thermoelectric materials convert heat into electrical energy via Seebeck effect [**44**]. A material with high electrical conductivity (σ/τ), Seebeck coefficients (S) and figure of merit (ZT), and low thermal conductivity (κ/τ) is considered to be suitable for thermoelectric power generation. In present case, our calculated κ/τ with its electronic ($\kappa_e/\tau$) and the lattice ($\kappa_L/\tau$) contribution, σ/τ for $Rb_2TeBr_6$ and $Cs_2TeBr_6$ are shown in **Fig. 6**. Whereas, computed S, carrier concentration (n) and ZT are depicted in **Fig. 7**.

The computed ($\kappa_e/\tau$) for the $Rb_2TeBr_6$ and $Cs_2TeBr_6$ compounds is shown in **Fig. 6 (a)** while $\kappa_L/\tau$ calculated through slack equation [**45**] is plotted in **Fig 6 (b)**. These figures summarize that phonon (electron) contribution toward heat transfer decreases (increase) with increase in temperature. To study overall effect of heat transfer, the $\kappa_e/\tau$ and $\kappa_L/\tau$ are combined in **Fig 6 (c)** to total lattice thermal conductivity (κ/τ). This figure indicates that κ/τ decrease up to 350 K and then increase as temperature rises. On other side, the **Fig 6 (d)** approves the semiconductor

behavior of Rb/$Cs_2TeBr_6$ vacancy ordered double perovskites. Because the increase in temperature increases intrinsic carrier's concentration, this turns an increase in electrical conductivity (σ/τ).

The temperature gradient in a material produces potential difference which is worth to note, because the ratio of potential difference and temperature gradients defines the S. Which can be quantum mechanically expressed as [46]

$$S = \left(\frac{8\pi^2}{3e}\right)\left(\frac{K_B^2}{h^2}\right)\left(\frac{\pi}{3n}\right)^{\frac{2}{3}} m^*T \qquad (4)$$

Where, n is carrier concentration, m* is carriers effective mass, $K_B$ represent Boltzmann constant and $h$ is plank constant. The computed S for Rb/$Cs_2TeBr_6$ perovskites is shown in **Fig. 7 (a)**. Where, S for both the compounds shows similar behavior. The value of S linearly decreases with increase in temperature. This is justified by the fact that S has inverse relation to n (eq. 4). **Fig. 7(b) shows** that value of n increases with the increase in temperature. This increase results a decrease in S of Rb/$Cs_2TeBr_6$ perovskites. Furthermore, the positive values of S explore Rb/$Cs_2TeBr_6$ perovskites as p-type semiconductors which are early predicted by DOS plots.

An important quantitative which characterize the thermoelectric effectiveness of a materials is its figure of merit (ZT). The calculated ZT versus temperature for Rb/$Cs_2TeBr_6$ perovskites is given in **Fig. 7 (c, d)**. These figures make it clear that ZT of both the compounds have also similar behavior. Up to 500 K the ZT values linearly increases with increase in temperature. Above this temperature, gradual changes have been seen in ZT. Maximum values of ZT were computed as 0.580 for $Cs_2TeBr_6$ and 0.578 for $Cs_2TeBr_6$ at 800 K. Our reported values of ZT will guide future studies.

## 4. Conclusions

This article described the structural, electronic, optical and thermoelectric properties of $Rb/Cs_2TeBr_6$, vacancy ordered double perovskites. The structural and electronic properties were compared with experimental and theoretical values available in scientific literature. From density of states plots it was found that the fundamental band gap lies between Br-$4p^5$ and $5p^4$ states of Te. Being the band gaps in visible region of electromagnetic spectrum, optical fitness of $Rb/Cs_2TeBr_6$ perovskites for solar cells was checked by calculating optical parameters such as real and imaginary parts of dielectric function, optical conductivity and reflectivity. The spectrum of these values within 0-6 eV confirmed maximum absorption of visible photons and maximum reflection of ultraviolet photons. This excellent behavior proposed $Rb/Cs_2TeBr_6$ perovskites as best materials for solar cell fabrications. Furthermore, the computed values of Seebeck coefficients and figure of merit confirmed the effectiveness of studied perovskites for thermoelectric power generation.

**References**


1. E. Yang, X. Lao, Solar Energy 207 (2020) 165–172
2. Z. Li, M. Yang, Ji-Sang Park, Su-Huai Wie, J. J. Berry, K. Zhu, Chem. Mater. 28 (2016) 284−292
3. M. Aslam, A. Khan, M. A. Hasmi, M. Sajjad, E. Algrafy, G. M. Mustafa, A. Mahmmod, S. M. Ramay, J Mater Res Technol. 9 (2020) 9965-9971
4. Best Research-Cell Efficiency Chart. https://www.nrel.gov/pv/cell-efficiency.html (2019).
5. Q. F. Dong, et al. Science 347 (2015) 967–970
6. Shi, D. et al. Science 347 (2015) 519–522.

7. Q. Chen, C. Zhang, M. Zhu, S. Liu, M. E. Siemens, S. Gu, J. Zhu, J. Shen, X. Wu, C. Liao, J. Zhang, X. Wang, M. Xiao, Appl. Phys. Lett. 108 (**2016**) 081902
8. S. Saini, A. Baranwal, T. Yabuki, S. Hayase, K. Miyazaki, MRS Adv. 4 (2019) 1719–1725
9. Y. P. He, G. Galli, Chem. Mater 26 (2014)5394–5400
10. A. Filippetti, C. Caddeo, P. Delugas, A. Mattoni, *J. Phys. Chem. C*, 120 (2016) 28472–28479
11. D. B. Mitzi, C. A. Feild, W. T. A. Harrison, A. M. Guloy, Nature 369 (1994) 467–469.
12. L. Tianjun, Z. Xiaoming, L. Jianwei, L. Zilu, L. Fabiola, M. Silvia, B. C. Schroeder, O. Fenwick, Nature Communications 10 (2019) 5750
13. Y. Takahashi, H. Hasegawa, Y. Takahashi, T. Inabe,. J. Solid State Chem. 205 (2013) 39–43
14. B. Lee, C. C. Stoumpos, N. J. Zhou, F. Hao, C. Malliakas, C. Y. Yeh, T. J.Marks, M. G. Kanatzidis, R. P. H Chang,. Journal of the American Chemical Society 136 (2014) 15379 - 15385
15. A. E. Maughan, A. M. Ganose, M. M. Bordelon, E. M. Miller, D. O. Scanlon, J. R. Neilson, Journal of the American Chemical Society 138 (2016) 8453–8464
16. G. Murtaza, S. Hussain, M. Faizan, S. Khan, E. Algrafy, M. A. Ali, A. Laref, Physica B 595 (2020) 412345
17. Q. Mahmood, T. Gharib, A. Rached, A. Laref, M. A. Kamran, Mat. Sci. Semicond. Proc. 112 (2020) 105009
18. B. Lee, A. Krenselewski, S. I. Baik, D. N. Seidman, R. P. H. Chang, Sustainable Energy & Fuels 1 (4) (2017) 710-724.
19. G. Kapil, T. Ohta,; T. Koyanagi, M. Vigneshwaran, Y. H. Zhang, Y. Ogomi, S. S. Pandey, K. Yoshino, Q. Shen, T. Toyoda, M. M. Rahman, T. Minemoto, T. N. Murakami, H. Segawa, S. Hayase, Journal of Physical Chemistry C 121 (2017) 13092-13100.
20. R. Ullah, M. A. Ali, G. Murtaza, A. Mahmood, S. M. Ramay, Int J Energy Res. 2020; 1–13. https://doi.org/10.1002/er.5638
21. Abriel, W.; Ihringer, J. *J. Solid State Chem.* **1984**, *52*, 274–280.
22. Abriel, W. *Z. Naturforsch., Anorg. Chem. Org. Chem* **1987**, *42*, 1273–1281
23. M.N. Amar, M.A. Ghriga, M.E.A.B. Seghier, H. Ouaer J. Phys. Chem. B 124 (2020) 6037–6045
24. M.G. Brik, I.V.Kityk Journal of Physics and Chemistry of Solids 72 (2011) 1256–1260
25. V. Sidey, Journal of Physics and Chemistry of Solids 126 (2019) 310–313

26. E. Yu. Peresh, O. V. Zubaka, S. V. Kun, I. V. Galagovets, I. E. Barchii, M. Yu. Sabov, Inorganic Materials 37 (2001) 849-852
27. M. A. Ali, A. Khan, S. H. Khan, T Ouohrani , G Murtaza, R. Khenata, S. B. Omran, Mat. Sci. Semicond. Proc. 38 (2015) 57
28. P. Bhala, K. Schwarz, F. Tran, R. Laskowski, G. K. H. Madsen, D. L. Marks, J. Chem. Phys. 152 (2020) 074101
29. Z. Wu, R. E. Cohen Phys. Rev. B 73 (2006) 235116.
30. E. Engle, S. H. Vosko, Phys. Rev. B 47 (1993) 13164
31. F. Tran, P. Blaha, Physical review letters 102 (2009) 226401.
32. G. K. H. Madsen, , D. J. Singh, Computer Physics Communications 175 (2006) 67-71
33. H. J. Monkhorst, J. D. Pack Phys. Rev. B, 13 (1976) 5188.
34. J. Breternitz,; S. Schorr, Adv. Energy Mater. 8 (2018) 1802366.
35. C. J. Bartel, C. Sutton, B. R. Goldsmith, R. Ouyang, C. B. Musgrave, L. M. Chiringhelli, M. Scheffler, Sci. Adv. 5 (2019) eaav0693
36. M.A. Ali, G. Murtaza, A. Laref, Chin Phys B. 29 (2020) 066102.
37. F.D. Murnaghan, *Proc. Natl. Acad. Sci. USA* **30** (1944) 244.
38. L. He, F. Liu, G. Hautier, M.J.T Oliveira, M.A.L. Marques, F.D. Vila, J. J. Rehr, G. Rignanese, A. Zhou, Phys. Rev. B 89 (2014) 064305
39. Q. Mahmood, M. Yaseen, M. Hassan, M.S. Rashid, I. Tlili, A. Laref, Mater. Res. Express 6 (2019) 045901
40. J. A. Abrahem, Int. J. Mod. Phys. B 33 (2019) 1950314
41. G. Murtaza, I. Ahmad, Physica B: Condensed Matter, 406 (2011) 3222
42. M. Huma, M. Rashid, Q. Mahmood, E. Algrafy, N. A. Kattan, A. Laref, A. S. Bhatti, Mat. Sci. Semicond. Proc. 121 (2021) 105313
43. M. A. Ali, H. Aleem, B. Sarwar, G. Murtaza Indian J Phys 94 (2020) 477-484
44. E. Haque, M. A. Hossain, Computational Condensed Matter 16 (2019) e00374
45. G. A. Slack, *J. Phys. Chem. Solids* **34** (1973) 321–335
46. S. Yousaf , D. C. Gupta, Mater Chem Phys. 192 (2017) 33-40

## Figures caption

**Fig. 1** The (**a**) convensional and (**b**) primitive uni cell of Rb/$Cs_2TeBr_6$ perovskites

**Fig. 2** The volume optimization curves for Rb/$Cs_2TeBr_6$ perovskites

**Fig. 3** Calculated band structures of Rb/$Cs_2TeBr_6$ perovskites through WC-GGA, EV-GGA and MBJ

**Fig. 4** Density of states for Rb/$Cs_2TeBr_6$ vacancy ordered double perovskites

**Fig. 5** Calculated (a) real $\varepsilon_1(\omega)$ and (b) imaginary $\varepsilon_2(\omega)$ parts of dielectric function, (c) optical conductivity $\sigma(\omega)$ and (d) reflectivity $R(\omega)$ for Rb/$Cs_2TeBr_6$ perovskites

**Fig. 6** Temperature dependent (a) electronic, $\kappa_e/\tau$ (b) lattice, $\kappa_L/\tau$ and (c) total, $\kappa/\tau$ thermal conductivity and (d) electrical conductivity ($\sigma/\tau$) of Rb/$Cs_2TeBr_6$ perovskites

**Fig. 7** (a) Seebeck coefficient, S (b) carrier concentration (n) of Rb/$Cs_2TeBr_6$ perovskites and Figure of merit, ZT of (c) $Rb_2TeBr_6$ and (d) $Cs_2TeBr_6$ at different temperatures

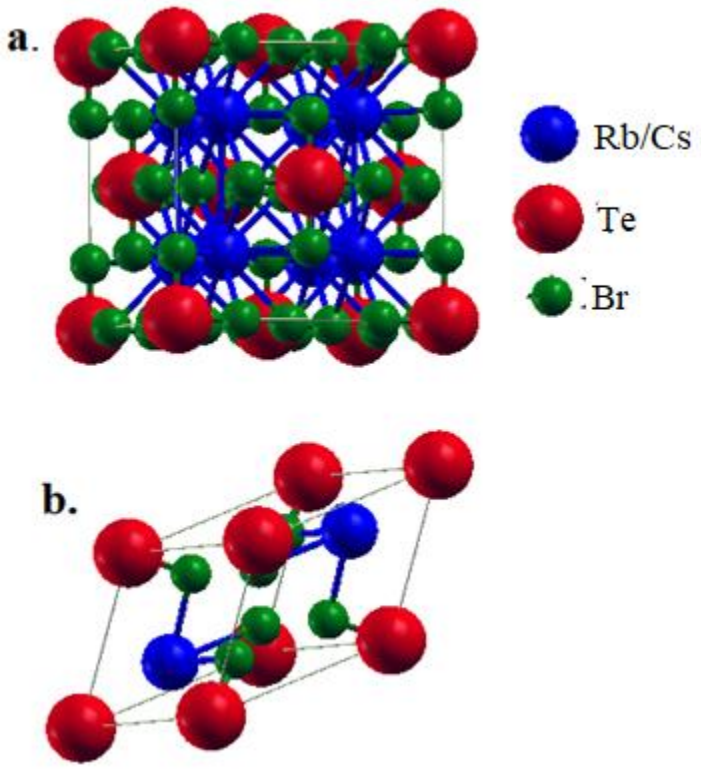


***Figure 1***

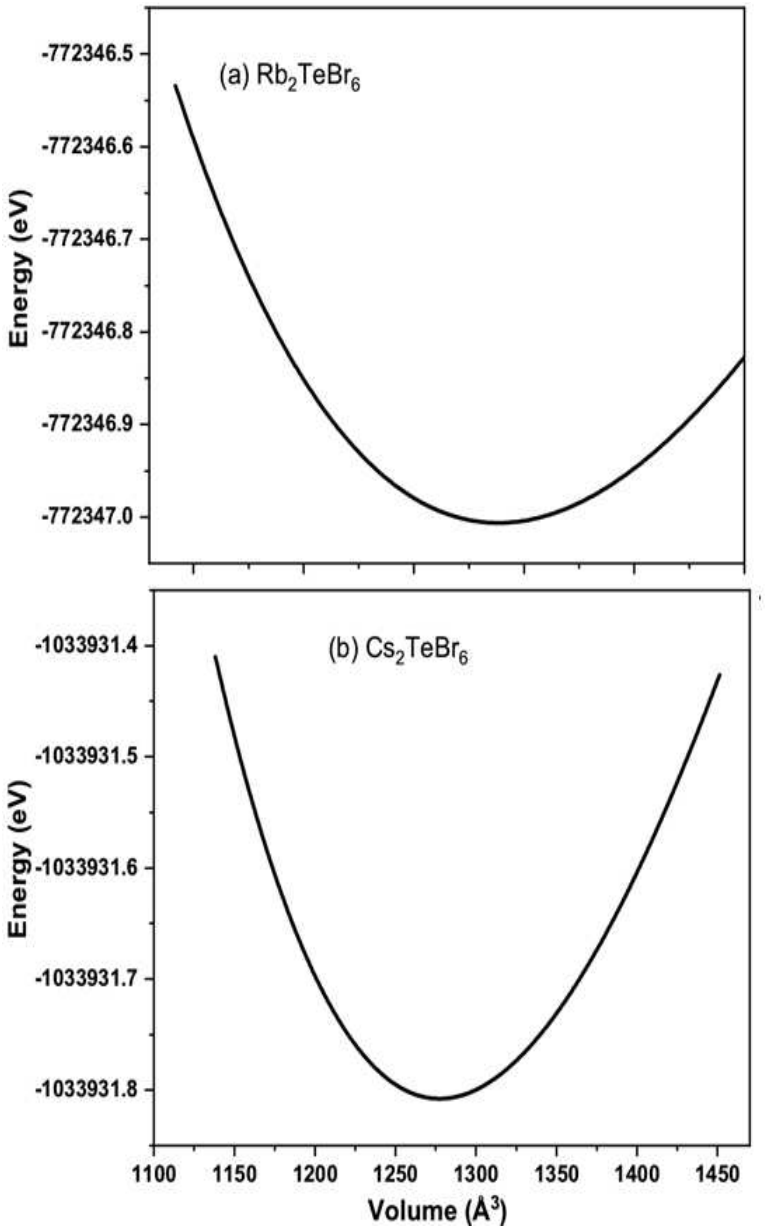
(a) $Rb_2TeBr_6$
Energy (eV)
-772346.5
-772346.6
-772346.7
-772346.8
-772346.9
-772347.0
(b) $Cs_2TeBr_6$
Energy (eV)
-1033931.4
-1033931.5
-1033931.6
-1033931.7
-1033931.8
1100
1150
1200
1250
1300
1350
1400
1450
Volume (Å$^3$)

***Figure 2***

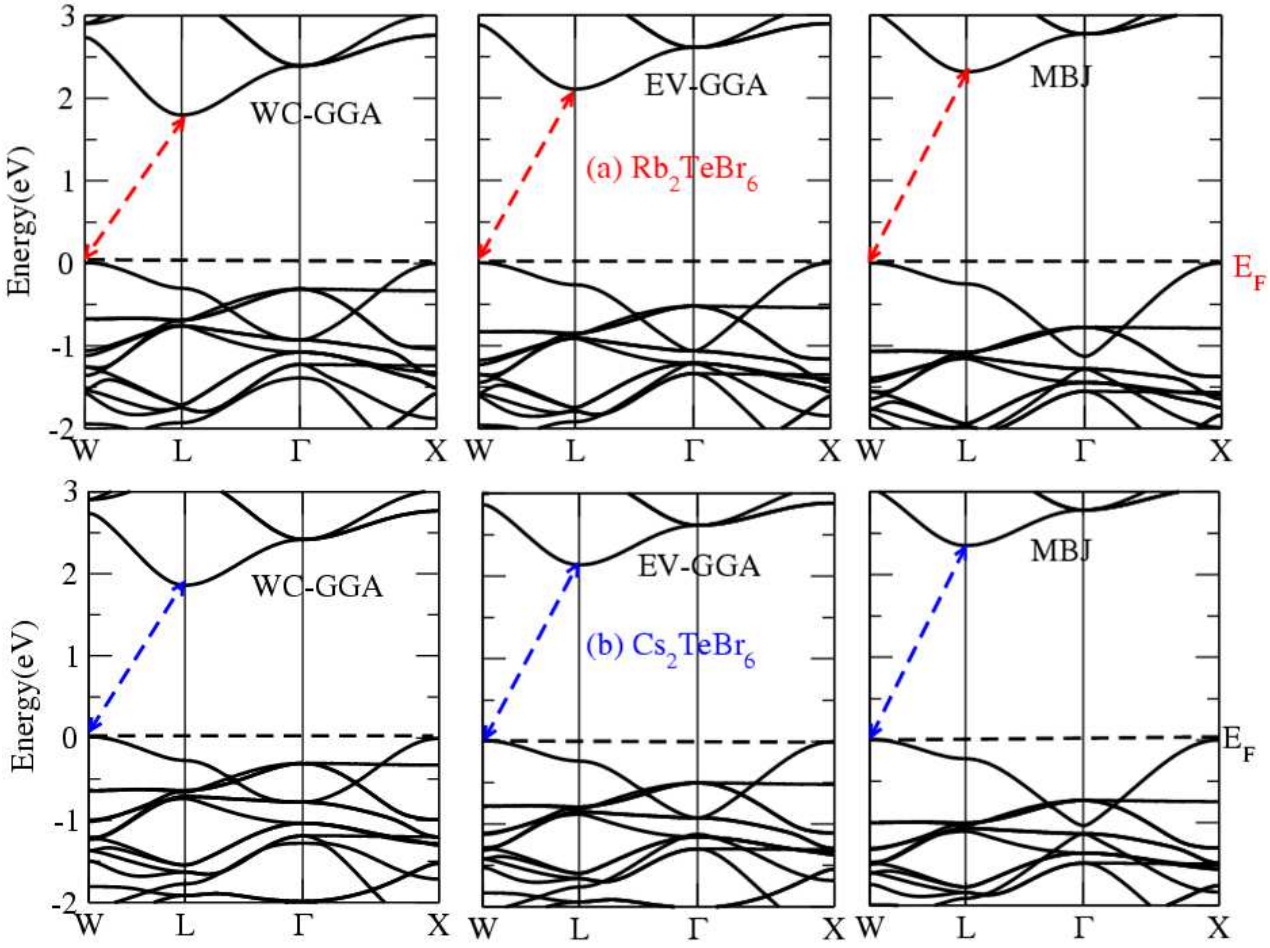


***Figure 3***

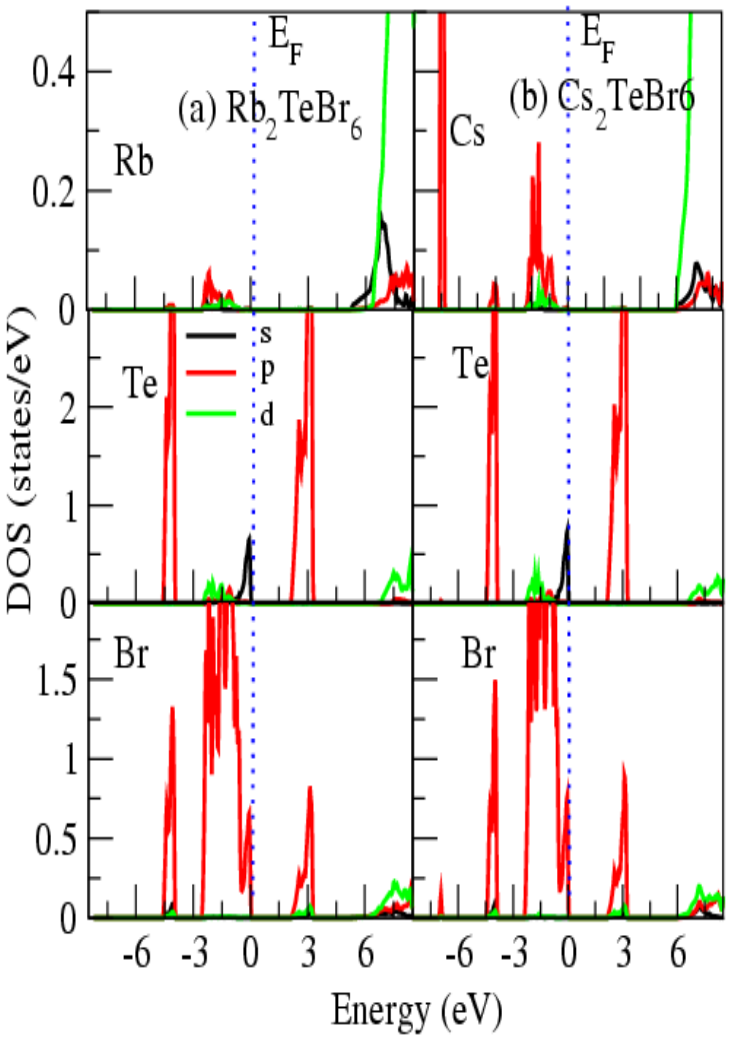
E_F
(a) Rb2TeBr6
Rb
Cs
(b) Cs2TeBr6
Te
Br
s
p
d
DOS (states/eV)
Energy (eV)

***Figure 4***

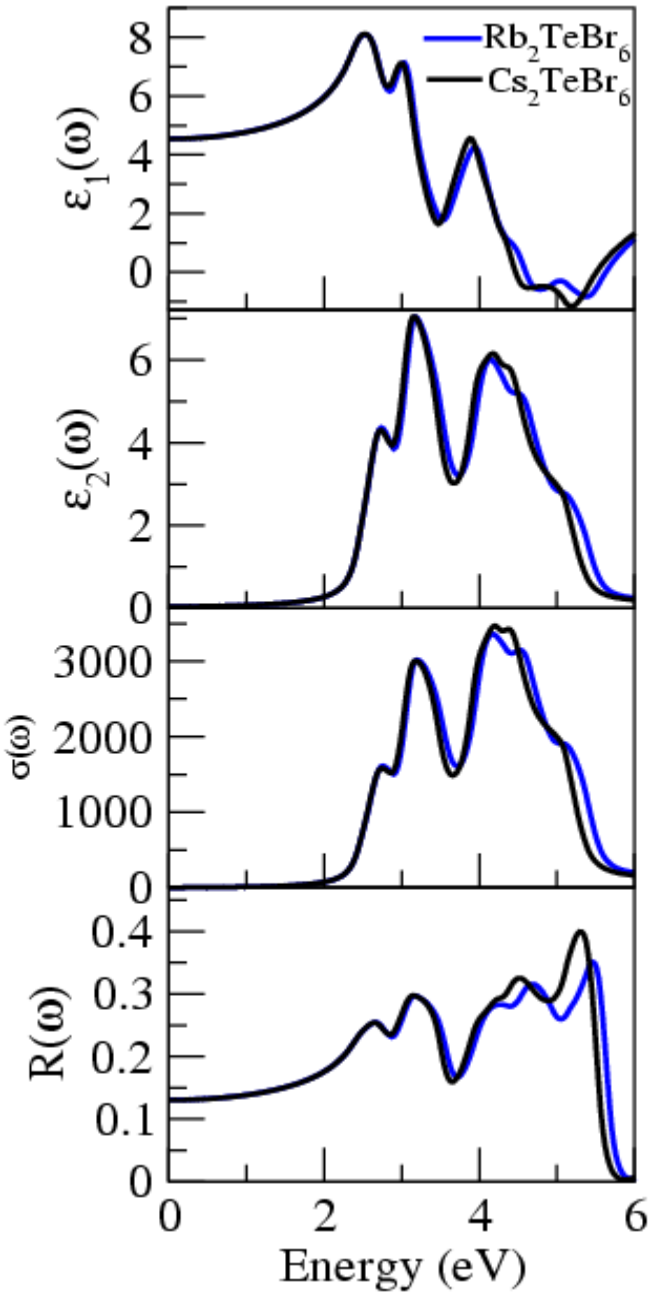


***Figure 5***

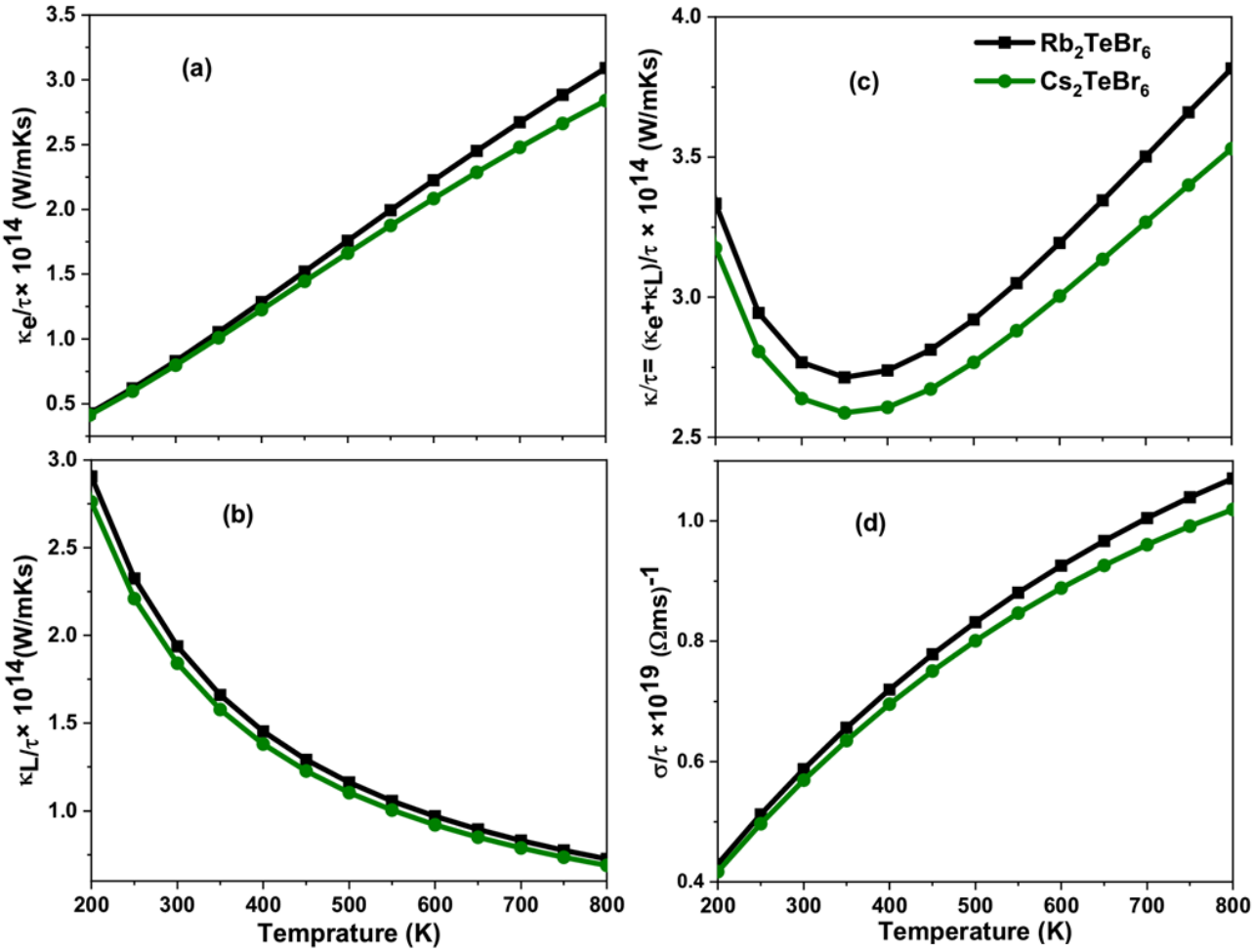
(a)
(b)
(c)
(d)
$\kappa_e/\tau \times 10^{14}$ (W/mKs)
$\kappa_L/\tau \times 10^{14}$ (W/mKs)
$\kappa/\tau = (\kappa_e+\kappa_L)/\tau \times 10^{14}$ (W/mKs)
$\sigma/\tau \times 10^{19}$ $(\Omega ms)^{-1}$
Temprature (K)
Temperature (K)
$Rb_2TeBr_6$
$Cs_2TeBr_6$

*Figure 6*

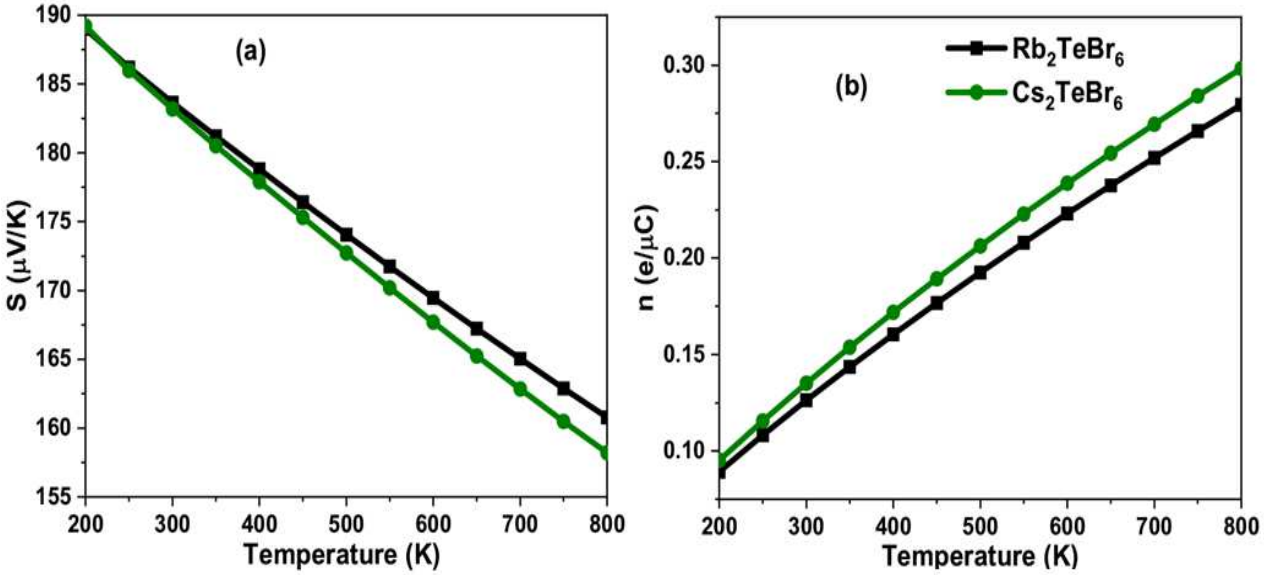


*Figure 7*

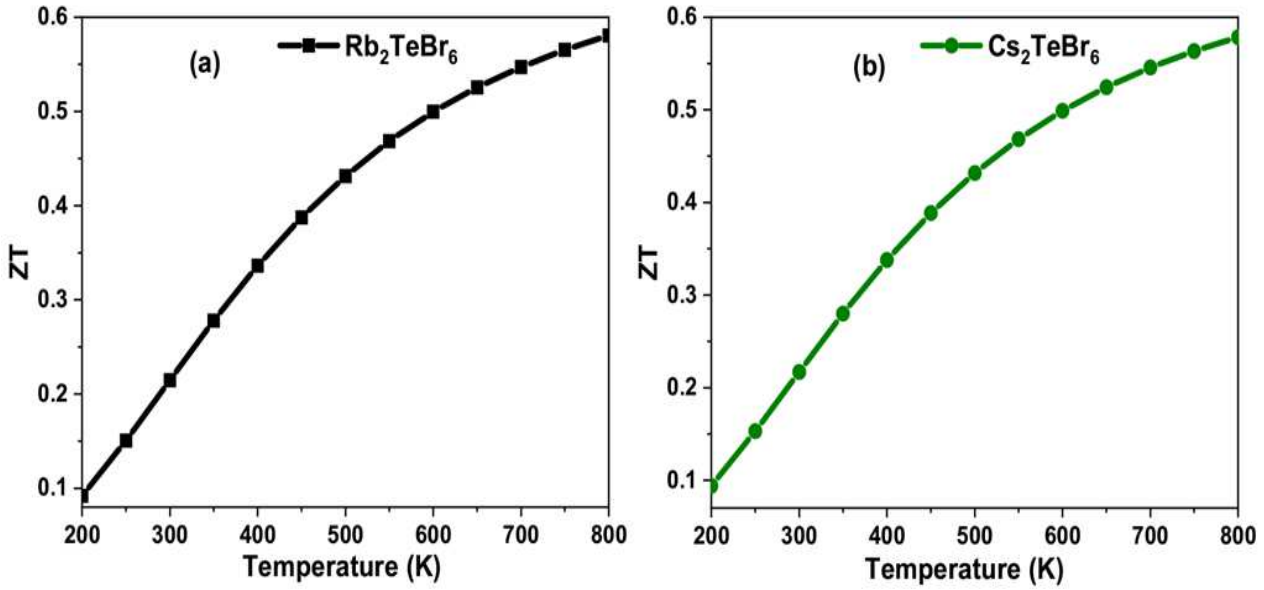


*Figure 7*

**Table 1** Optimized atomic positions of $Rb_2TeBr_6$ and $Cs_2TeBr_6$

| Atom | Positions | | |
|---|---|---|---|
| | x | y | z |
| **$Rb_2TeBr_6$** | | | |
| **Rb** | 0.25 | 0.25 | 0.25 |
| **Rb** | 0.25 | 0.25 | 0.75 |
| **Te** | 0 | 0 | 0 |
| **Br1** | 0 | 0 | 0.25272951 |
| **Br2** | 0 | 0 | 0.74727049 |
| **Br3** | 0 | 0.25272951 | 0 |
| **Br4** | 0 | 0.74727049 | 0 |
| **Br5** | 0.25272951 | 0 | 0 |
| **Br6** | 0.74727049 | 0 | 0 |
| **$Cs_2TeBr_6$** | | | |
| **Cs** | 0.25 | 0.25 | 0.25 |
| **Cs** | 0.25 | 0.25 | 0.75 |
| **Te** | 0 | 0 | 0 |
| **Br1** | 0 | 0 | 025118388 |
| **Br2** | 0 | 0 | 0.74881612 |
| **Br3** | 0 | 025118388 | 0 |
| **Br4** | 0 | 0.74881612 | 0 |
| **Br5** | 0.74881612 | 0 | 0 |
| **Br6** | 0.74881612 | 0 | 0 |

**Table 2** The ground state energies of bulk Cs, Se, Te, and Cl atoms and Rb/$Cs_2TeBr_6$ perovskites with formation energies in eV

| Parameter | $Rb_2TeBr_6$ | $Cs_2TeBr_6$ |
|---|---|---|
| $E_{Cs/Rb}$ | -81080.61 | -211873.32 |
| $E_{Te}$ | -184853.11 | -184853.11 |
| $E_{Br}$ | -70885.37 | -70885.37 |
| $E(Rb_2/Cs_2TeBr_6)$ | -772347.01 | -1033931.81 |
| $E\ (F)$ | -20.46 | -19.4 |

**Table 3** The calculated values of lattice parameter ($a_\circ$), Volume (V), Bulk modulus (B) through WC-GGA with available experimental and theoretical results

| **Parameter** | | **$Rb_2TeBr_6$** | **$Cs_2TeBr_6$** |
|---|---|---|---|
| **$a_\circ$ (Å)** | This | 10.7433 | 10.8549 |
| | Exp. | 10.713 [**21**] | 10.873 [**22**] |
| | Theo. | 10.719 [**23**]<br>10.743 [**24**]<br>10.651[**25**] | 10.874 [**23**]<br>11.043 [**24**] |
| **V ($Å^3$)** | | 1238.42 | 1277.41 |
| **B (GPa)** | | 27.08 | 26.64 |

**Table 4** The calculated band gaps through WC-GGA, EV-GGA and MBJ with experimental results

| **Band gap** | **Method** | **$Rb_2TeBr_6$** | **$Cs_2TeBr_6$** |
|---|---|---|---|
| **This** | WC-GGA | 1.77 | 1.83 |
| | EV-GGA | 2.09 | 2.10 |
| | MBJ | 2.31 | 2.33 |
| **Exp.** | | 2.14 [**26**] | 2.12 [**26**] |

# Figures

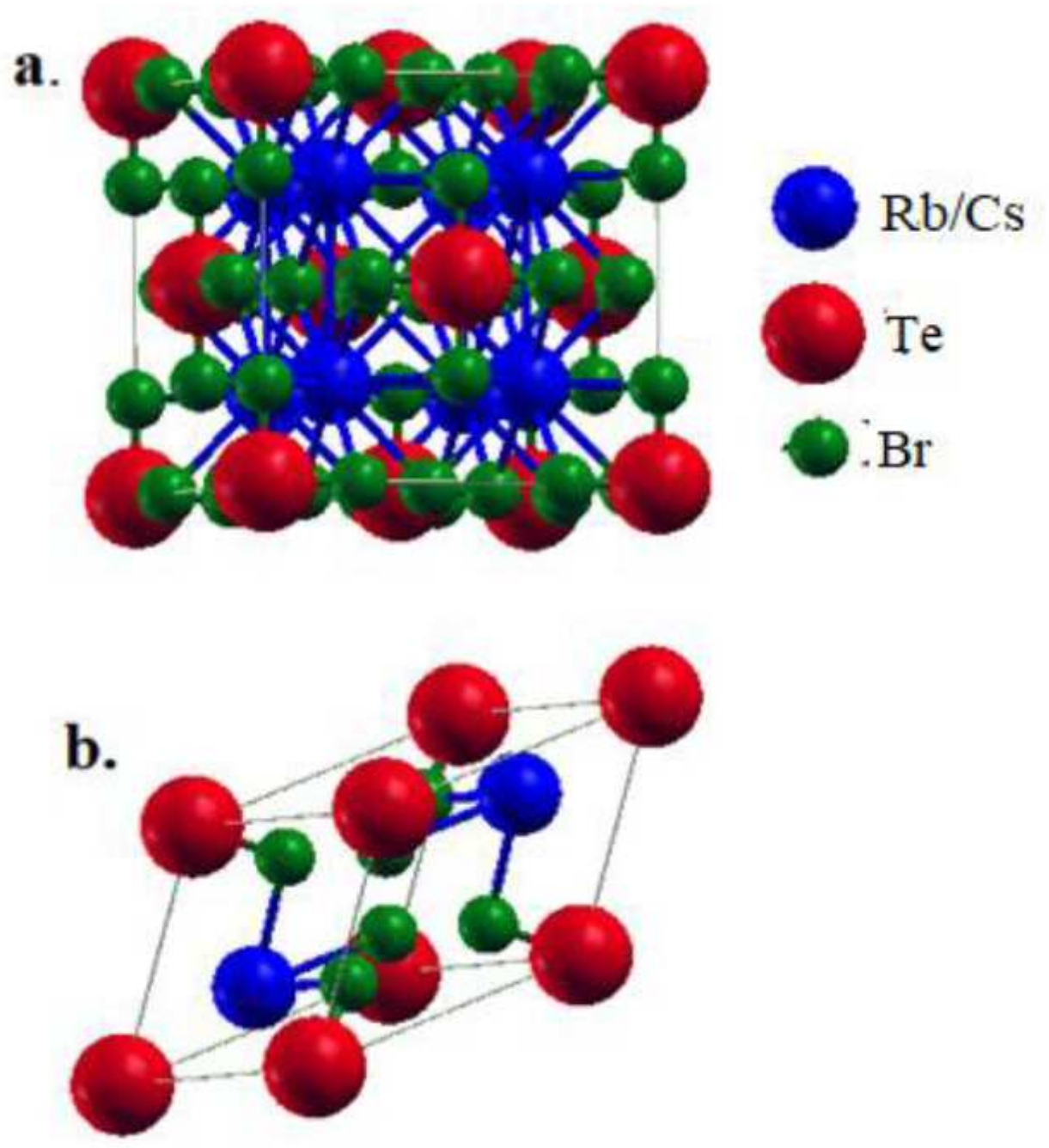


**Figure 1**

The (a) convensional and (b) primitive uni cell of Rb/Cs2TeBr6 perovskites

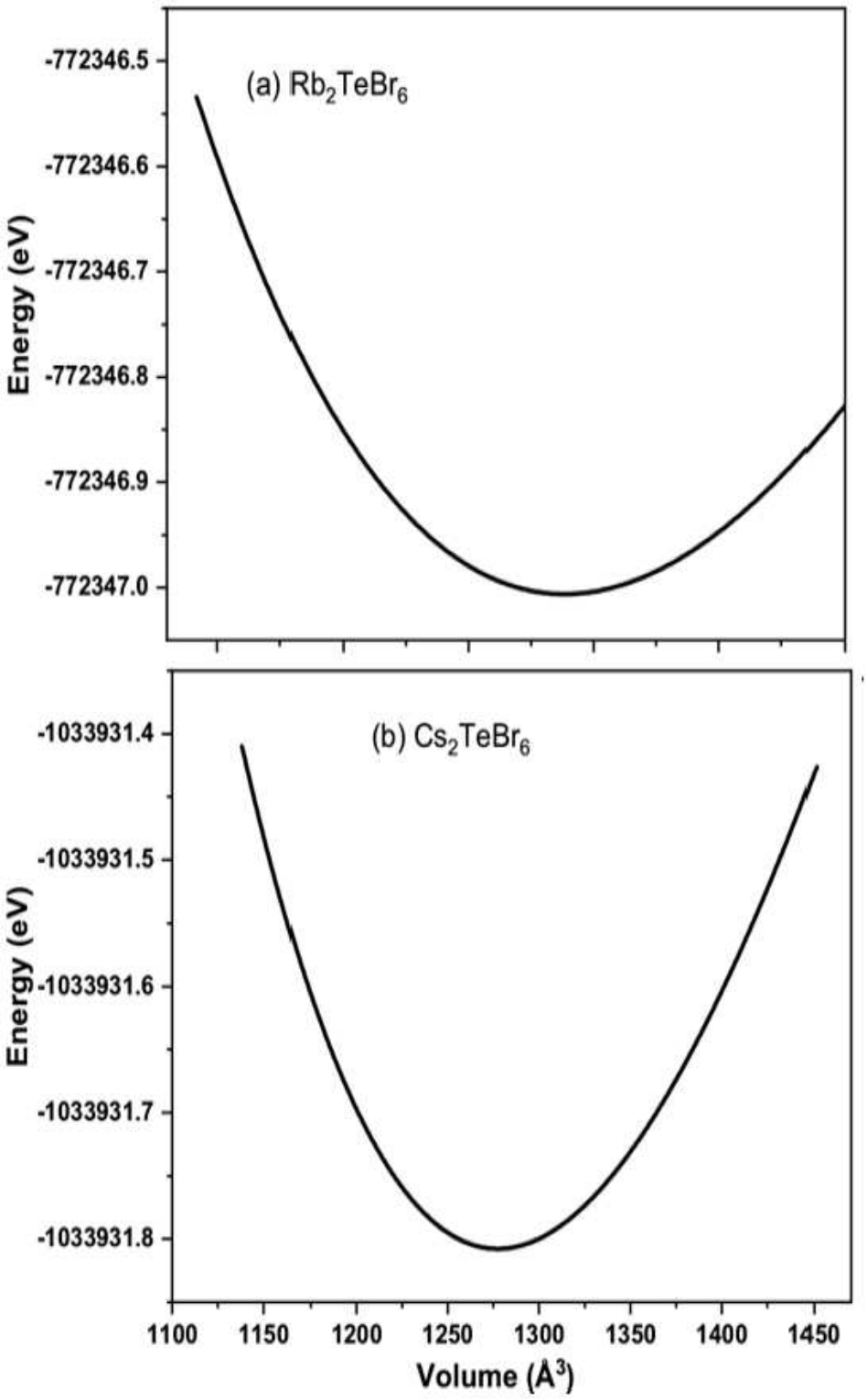


**Figure 2**

The volume optimization curves for Rb/Cs2TeBr6 perovskites

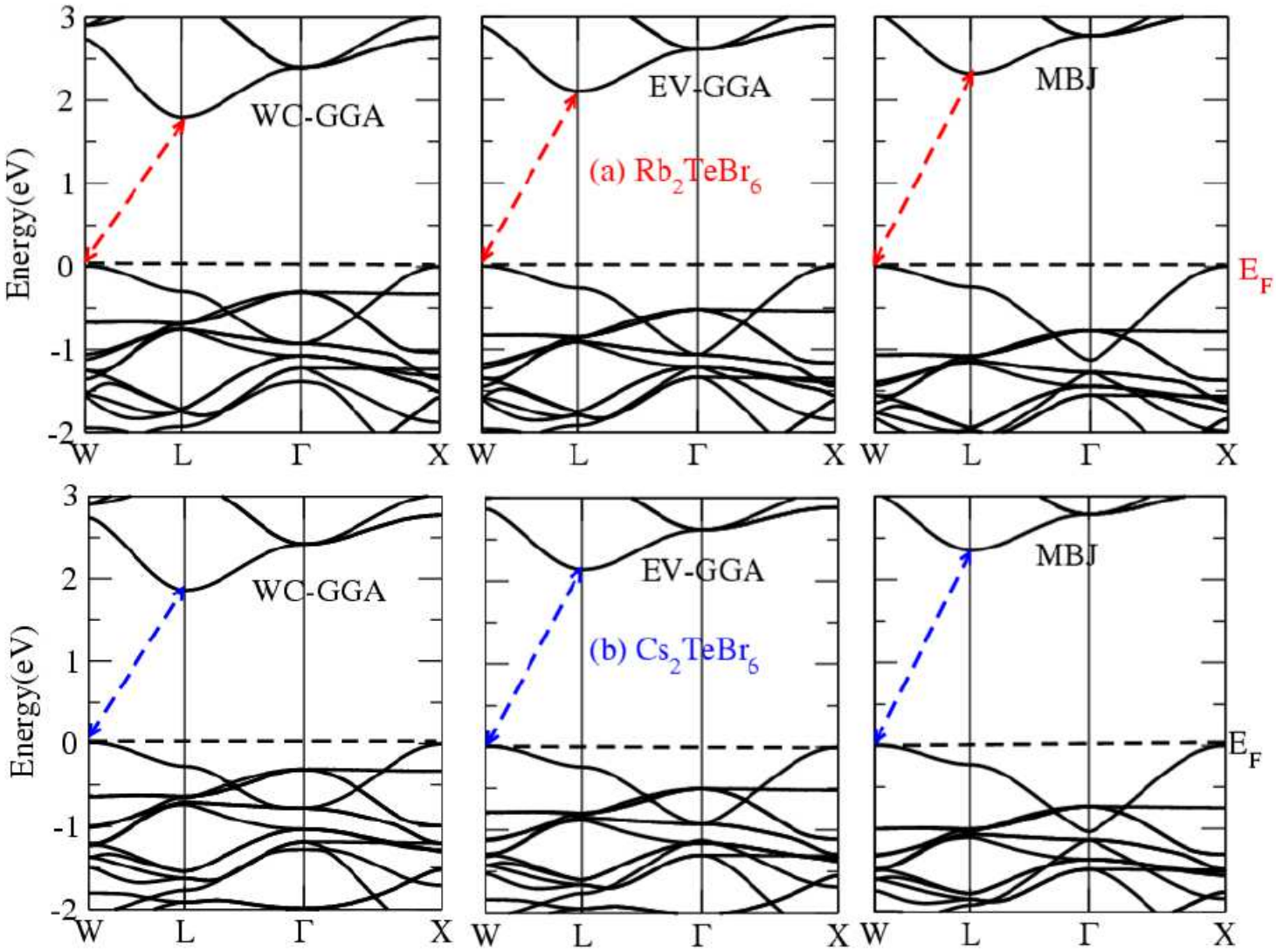


**Figure 3**

Calculated band structures of Rb/Cs2TeBr6 perovskites through WC-GGA, EV-GGA and MBJ

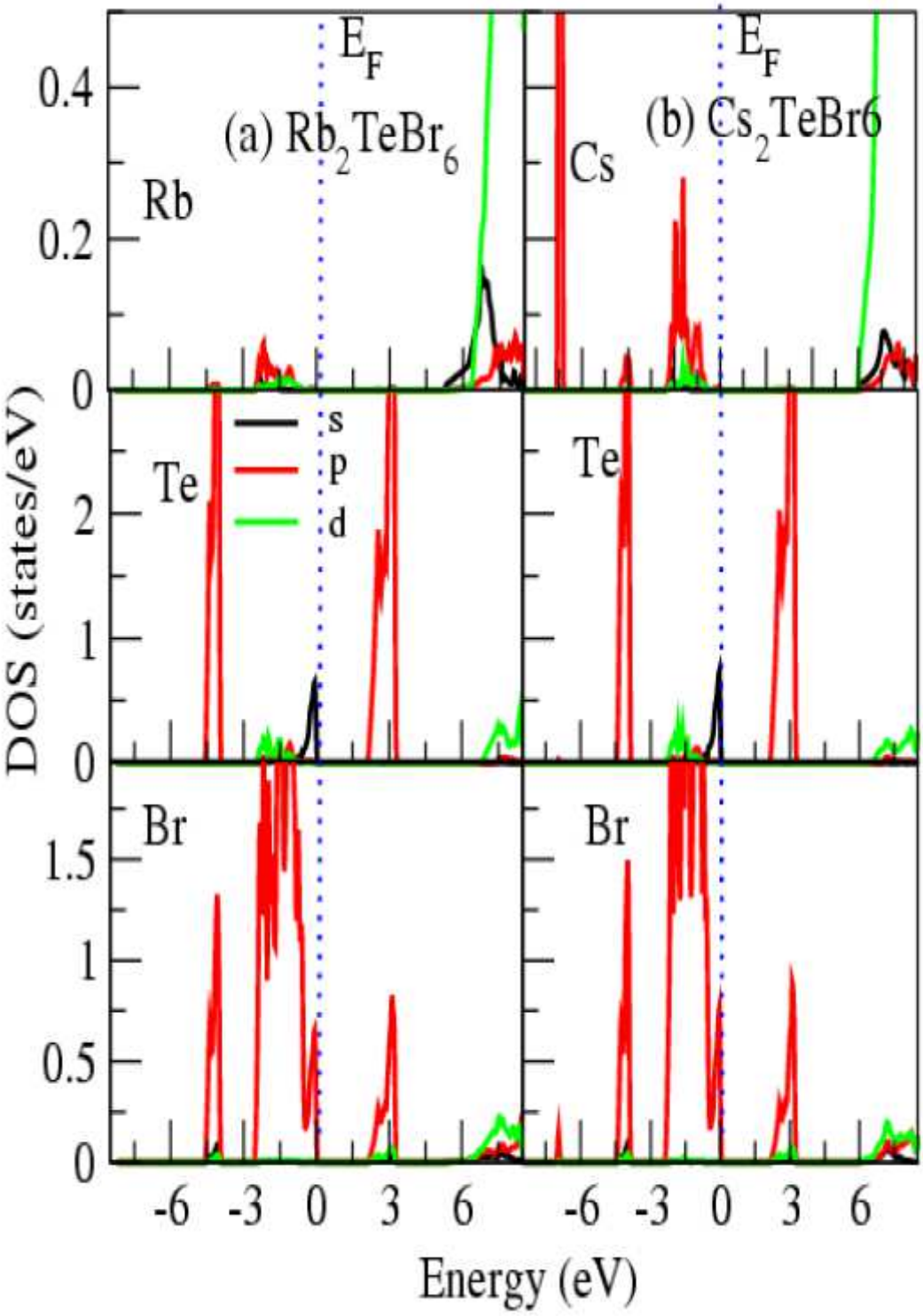


**Figure 4**

Density of states for Rb/Cs2TeBr6 vacancy ordered double perovskites

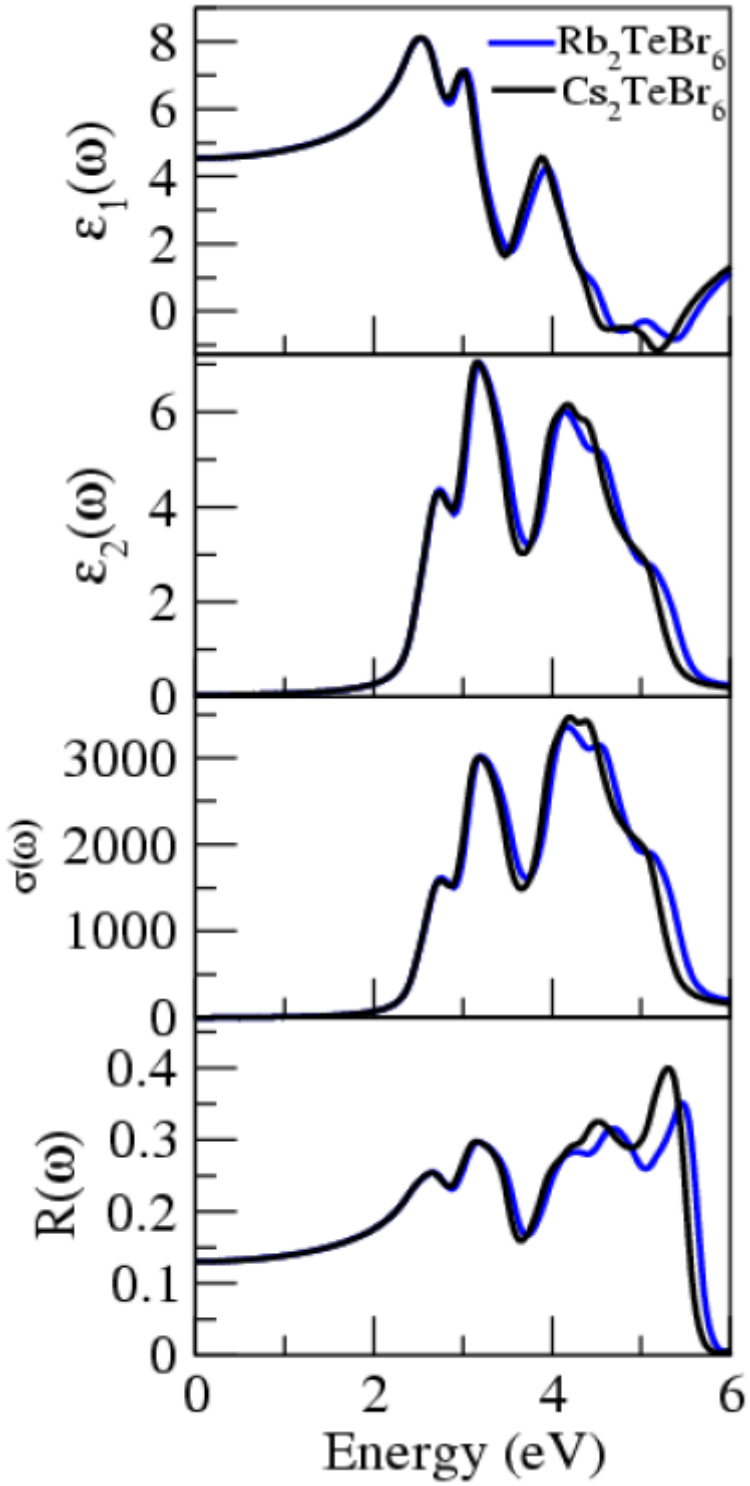


**Figure 5**

Calculated (a) real 1(ω) and (b) imaginary 2(ω) parts of dielectric function, (c) optical conductivity σ (ω) and (d) reflectivity R(ω) for Rb/Cs2TeBr6 perovskites

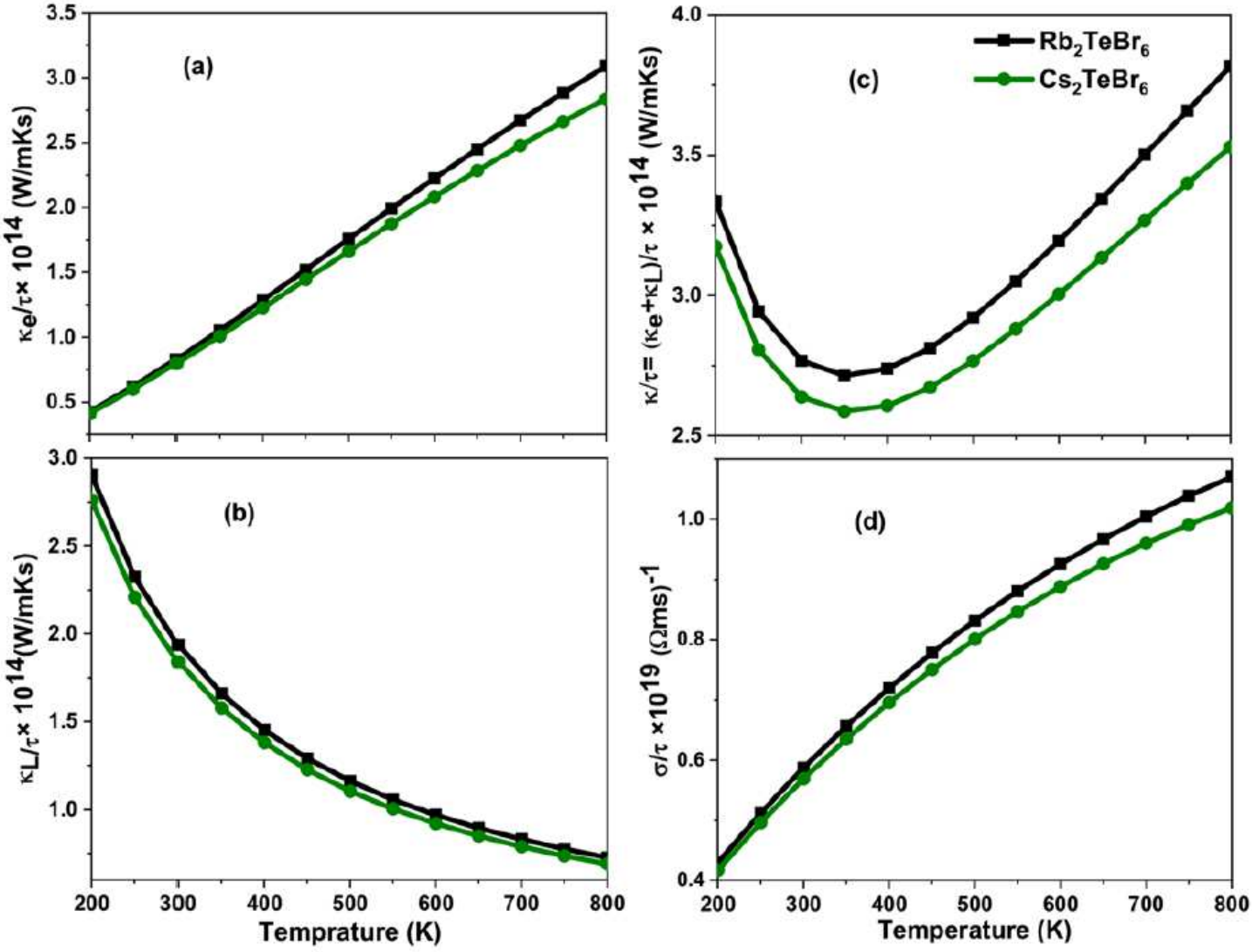


## Figure 6

Temperature dependent (a) electronic, κe/τ (b) lattice, κL/τ and (c) total, κ/τ thermal conductivity and (d) electrical conductivity (σ/τ) of Rb/Cs2TeBr6 perovskites

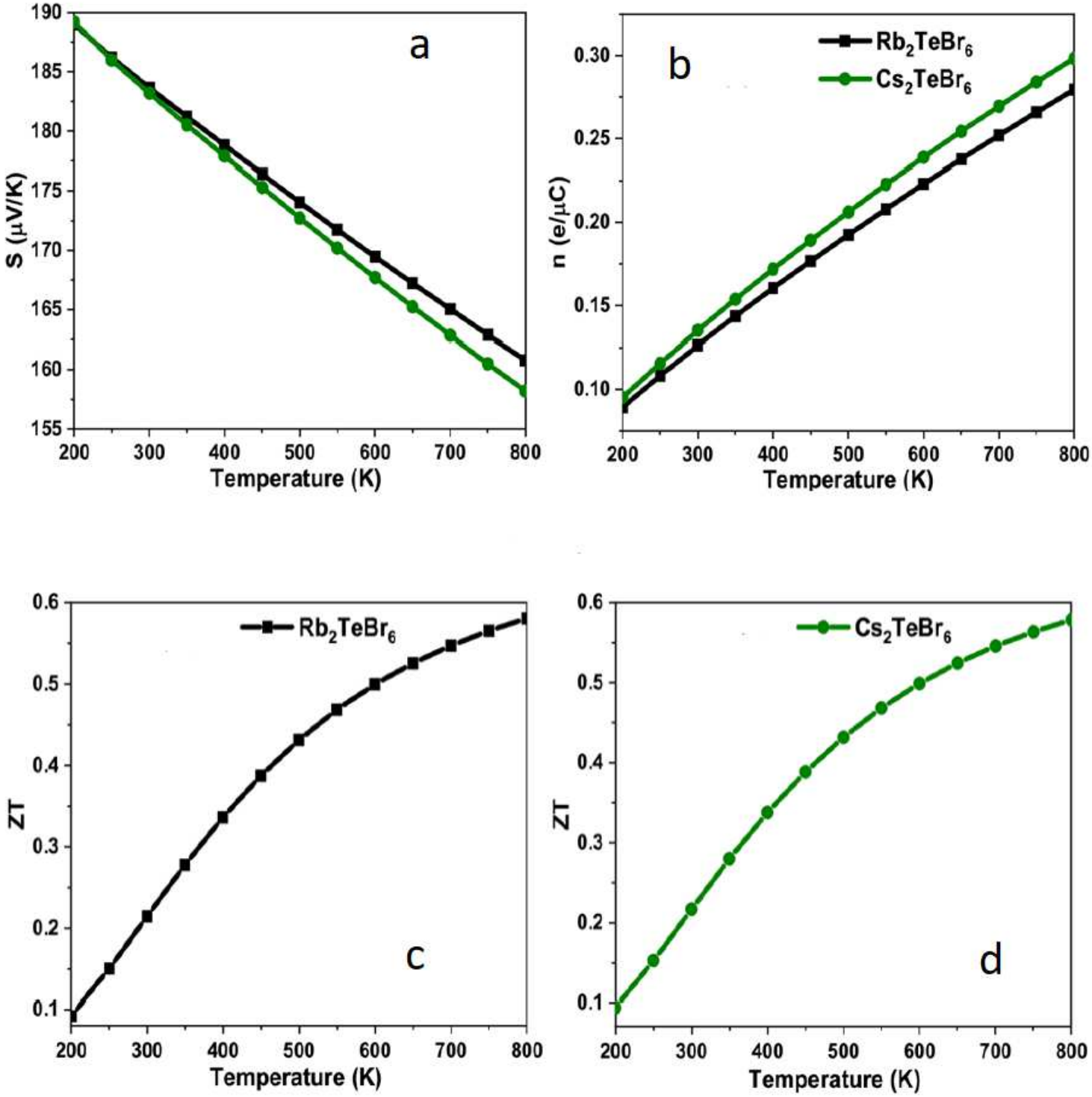


Figure 7

(a) Seebeck coefficient, S (b) carrier concentration (n) of Rb/Cs2TeBr6 perovskites and Figure of merit, ZT of (c) Rb2TeBr6 and (d) Cs2TeBr6 at different temperatures